Journal of Applied Sciences

ISSN 1812-5654

science alert

ANSInet
an open access publisher
http://ansinet.com

Journal of Applied Sciences 11 (22): 3698-3707, 2011
ISSN 1812-5654 / DOI: 10.3923/jas.2011.3698.3707

Prediction of Cutting Temperatures in Turning Carbon Fiber Reinforced Plastics Composites with Worn Tools

Chung-Shin Chang, Je-Ee Ho, Chang-Hu Chan and Baw-Chiang Hwang
Department of Mechanical and Electro-Mechtronic Engineering,
National Ilan University, 260, Taiwan

Abstract: Temperatures of the carbide tip's surface when turning Carbon Fiber Reinforced Plastics (CFRP) with a worn main cutting edge tool is investigated. The frictional forces and heat generated in the basic cutting tools are calculated by using the measured cutting forces and the theoretical cutting analysis. The heat partition factor between the tip and chip is solved by using the inverse heat transfer analysis which utilizes temperature on the carbide tip's surface measured by infrared as the input. The carbide tip's surface temperature is determined by Finite Element Analysis (FEA) and compared with temperatures obtained from experimental measurements. Good agreement demonstrates the proposed model.

Key words: Cutting temperature, carbon fiber reinforced fiber, carbide tip's surface, turning, FEA

INTRODUCTION

Composite materials are ideal for structural applications where high strength to weight and stiffness-to-weight ratios are required by Hocheng *et al*. (1997). Ferreira *et al*. (2001) showed that turning experiments were observed with the performance of different tool materials like ceramics, cemented carbide, Cubic Boron Nitride (CBN) and diamond. Experimental results showed that only diamond tools are suitable for use in finishing turning. In rough turning, the carbide tools can be used in some retractions parameters. Machining characteristics of composites vary from metals due to the following reasons: (1) FRP is machinable in a limited range of temperature, (2) the low thermal conductivity causes heat build up in the cutting zone during machining operation, since, there is only little dissipation by the materials; (3) the difference in the coefficient of linear expansion between the matrix and the fiber gives rise to residual stresses and makes it difficult to attain high dimensional accuracy and (4) the change in physical properties by the absorption of fluids has to be considered while deciding to use a coolant by Malhotra (1990).

Cutting temperature is an important parameter in the analysis metal cutting process. Singamneni (2005) demonstrated the mixed finite and boundary element method (FEM) finally enables the estimation of the cutting temperatures which is a simple, efficient method, and at the same time it is quite easy to be implemented. Chang (2006a) showed a model to accurately predict the cutting force for turning of carbon fiber reinforced plastics composites using chamfered main cutting carbide tools. The objective of this paper is to set up an oblique cutting CFRP model to study three-dimensional cutting temperature for a sharp worn tool with a chamfered main cutting edge.

THEORETICAL ANALYSIS

Composite materials are mainly molded parts, which require machining, especially face turning, to obtain the desired dimensional tolerances. Bhatnagar *et al*. (1995) showed that in machining of Fiber Reinforced Plastic (FRP) composite laminates; it can be assumed that the shear plane in the matrix depends only on the fiber orientation and not on the tool geometry. The available reports on cutting temperature and associated influences are mostly related to applications involving chamfered main cutting edge carbide tools.

Shamoto and Altintas (1999) demonstrated that the mechanics of oblique cutting are defined by five expressions. Three of the expressions are obtained from the geometry of oblique cutting and the remaining two are derived by applying either maximum shear stress or minimum energy principle. Since temperature is of fundamental importance in CFRP cutting operations, many attempts have been made to predict it. Chang (2008) presented a model to predict the cutting temperatures in turning of glass-fiber-reinforced plastics with chamfered main cutting edge sharp worn tools, that can accurately

Corresponding Author: Chung-Shin Chang, Department of Mechanical and Electro-Mechtronic Engineering,
National Ilan University, 260, Taiwan

Table 1: Tool geometry specifications (chamfered main cutting edge)

Side cutting edge angle C_s	Tool No.	Side rake angles α_{S1}, α_{S2} (α_{r1}, α_{r2})	Nose roundness (R)	Carbide tool
20°	1	10°, -10° (10°, -10°)	0.0, 0.1 (sharp and worn)	K10
20°	2	30°, -30° (30°, -30°)	0.0, 0.1 (sharp and worn)	K10
30°	3	10°, -10° (10°, -10°)	0.0, 0.1 (sharp and worn)	K10
30°	4	30°, -30° (30°, -30°)	0.0, 0.1 (sharp and worn)	K10
40°	5	10°, -10° (10°, -10°)	0.0, 0.1 (sharp and worn)	K10
40°	6	30°, -30° (30°, -30)	0.0, 0.1 (sharp and worn)	K10

Notation: Tool holder and tips

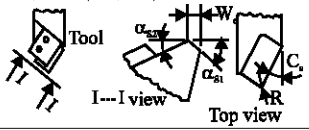

predict the cutting temperatures and the cutting forces. For the case of chamfered main cutting edge, temperatures and forces depend on nose radius R, worn depths d_B, cutting depth d, feed rate f, cutting speed V, first side rake angle α_{S1}, second side rake angle α_{S2} and parallel back rake angle α_b as shown in Table 1. The process for deriving the shear plane areas is divided into segments with tool wear and without wear.

- Shear area in the cutting process with chamfered cutting edge sharp tools without wear (Chang, 2006b)
- Shear area in the cutting process with chamfered cutting edge sharp tools considering wear

Takeyama and Murata (1963) showed that the mechanism of tool wear in turning can be classified into two basic types: (1) mechanical abrasion is directly proportional to the cutting distance and independent of the temperature and (2) physicochemical wear is considered to be a rate process closely associated with the temperature. For simplification, the wear effect of the tool edge is considered in the following such that the depth of tool wear t_W in the direction of cutting depths and geometrical wear angle φ_A on the tool face must be measured on line. Figure 2 and 3 reveal that the geometrical specification of tool wear on the tool face (triangle CNM) can be derived from the values of t_W and φ_A when already measured (Fig. 1, 2):

$$A = A_1+A_2+A_3+A_S \tag{1}$$

$$A_1 = 0.5a_3b_3\sin\theta_3 = 0.5a_3b_3 [1-(a_3^2+b_3^2-c_3^2)/2a_3b_3]^{1/2}\} (A_1 = \Delta NBE) \tag{2}$$

$$A_2 = \frac{1}{2}(a_4+b_4)\cdot h_4 \ (A_2 = \text{rectangle MDFE}') \tag{3}$$

$$A_3 = A_{31} + A_{32} \ (A_3 = \Delta ME'E + \Delta MNE) \tag{4}$$

$$A_{31} = \frac{a_5b_5}{2\cos\varphi_e}\sin\left(\frac{0.5\pi+\alpha_b-\angle A31}{2}\right) \tag{5}$$

$$\angle A31 = \cos^{-1}\left[\frac{c_5^2+d_5^2-e_5^2}{2c_5d_5}\right] \tag{6}$$

$$A_{32} = g_5h_5\frac{\sin(\angle A32)}{2\cos\varphi_e} \tag{7}$$

$$\angle A32 = \cos^{-1}\left[\frac{h_5^2+n_5^2-m_5^2}{2h_5n_5}\right] - \sin^{-1}\left[\frac{l_5}{s_5}\sin\left(\frac{\pi}{2}-\alpha_b\right)\right] \tag{8}$$

$$\angle A32 = \cos^{-1}\left[\frac{h_5^2+n_5^2-m_5^2}{2h_5n_5}\right] - \sin^{-1}\left[\frac{l_5}{s_5}\sin\left(\frac{\pi}{2}-\alpha_b\right)\right] \tag{9}$$

(A_S is the area of secondary chip :$\Delta D'\overline{Y}J$)

$$Q = Q_1+Q_2+Q_3 \tag{10}$$

$$Q_1 = \frac{0.5(d/\cos C_s - W_e\cos^2\alpha_{s1}\tan C_s)}{\cos\alpha_b}\cdot\frac{f\cos C_s - W_e\cos\alpha_{s1}}{\cos\alpha_{s2}} - (\overline{CN}\cdot\overline{NM}\sin\varphi_B)/0.5 \tag{11}$$

$$Q_2 = \frac{W_e\cos\alpha_{s1}(d/\cos C_{s1}\tan C_s)}{\cos\alpha_b} - \overline{CN}\cdot W_e\cos\alpha_{s1} \tag{12}$$

$$O_3 = (0.5W_e^2\cos\alpha_{s1}\tan C_s)/\cos\alpha_b \tag{13}$$

$$\overline{CM} = t_W(\cos C_S + \sin C_S\tan\varphi_A) \tag{14}$$

$$\overline{CN} = \frac{t_W(\cos C_S+\sin C_S\cdot\tan\varphi_A)}{(\sin\varphi_A\tan\varphi_A+\cos\varphi_B)} \tag{15}$$

$$\overline{NM} = (\overline{CM}^2+\overline{CN}^2-2\overline{CM}\cdot\overline{NM}\cos\varphi_B)^{1/2} \tag{16}$$

$$\angle CMN = \cos^{-1}\left[\frac{(\overline{CM}^2+\overline{CN}^2-\overline{NM}^2)}{2\overline{CM}\cdot\overline{CN}}\right] \tag{17}$$

$$\angle CNM = \cos^{-1}\left[\frac{(\overline{CN}^2+\overline{NM}^2-\overline{CM}^2)}{2\overline{CN}\cdot\overline{NM}}\right] \tag{18}$$

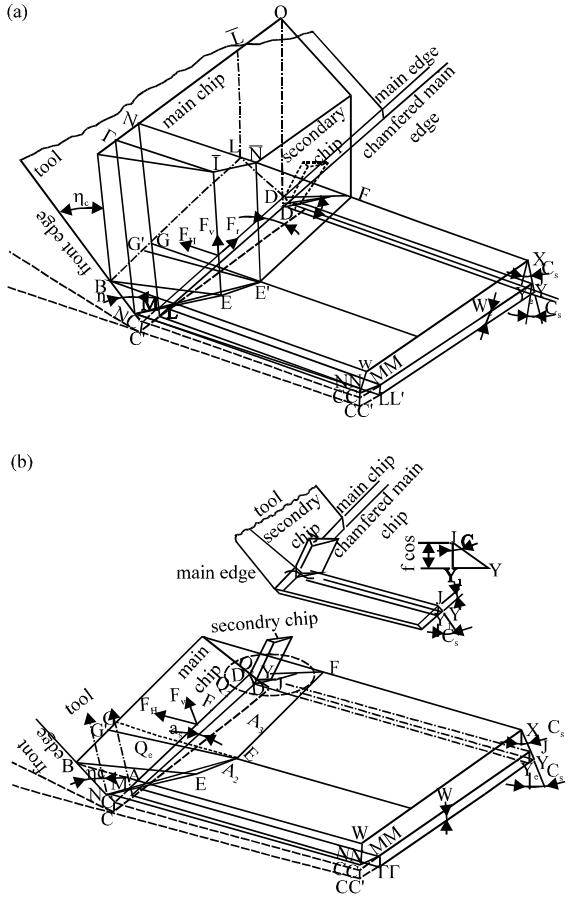

Fig. 1(a-b): (a) Basic and (b) detailed model of the chamfered main edge tool when wear (f>R, R ≠ 0)

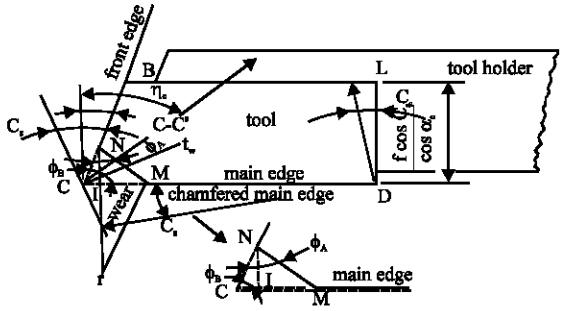

Fig. 2: Specifications of tool face with wear

Coefficients a_1, b_1, … h_2 a re shown in Appendix A; b_3, c_3, a_4, b_4, c_4 … r_5 are shown in Appendix B. The contact length of the tool edge can be considered as two types, as shown in Fig. 2, 3. Since, the distinction between types of contact length causes different cutting conditions, the shear plane areas with tool wear differs accordingly:

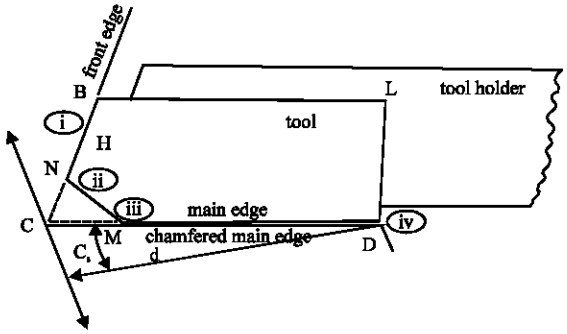

Fig. 3: Contact length L_f and L_P

$$\overline{NM}\cos\left(\frac{\pi}{2}-\angle CMN\right)<\left(\frac{f\cos C_s}{\cos\alpha_e}-W_e\cos\alpha_{s1}\right)$$

as shown in Fig. 2

From the above diagram, the contact length is:

$$l_f=\overline{HN}+\overline{NM}+\overline{MD}=\bar{i}\cdot\bar{ii}+\bar{ii}\cdot\bar{iii}+\bar{iii}\cdot\bar{iv}$$

$$\left[\frac{f\cos C_s/\cos\alpha_e)-W_e\cos\alpha_{s1})}{\cos(C_e-C_s)}+\overline{NM}+\frac{d}{\cos C_s\cos\alpha_b}-\overline{CM}\right] \quad (19)$$

Therefore, the projected contact length (l_p) on the projection line (i.e., on the plane of the work piece) is also derived:

$$l_p=\overline{HN}\cos C_e+\overline{NM}\cos(\angle CNM-C_e)+\overline{MD}\sin C_s$$
$$\left[\frac{f\cos C_s-W_e\cos\alpha_{s1})}{\cos\alpha_e\cos(C_e-C_s)}+\overline{NM}\cos(\angle CNM-C_e)+\right. \quad (20)$$
$$\left.(d/\cos C_s-\overline{CM})\sin C_s\right.$$

Energy method to predict cutting force: Wang *et al.* (1995) illustrated that the normal and shear forces along the fiber direction were calculated by assuming that the measured resultant force is equivalent to that present in the workpiece at the tool point. Transformation equations used to obtain the normal (N_s) and shear forces (F_s) along the fiber direction in terms of the principal (F_c) and thrust components (F_t) are shown in Eq. 21 and 22 (Wang *et al.*, 1995):

$$N_S=F_c\sin\theta+F_t\cos\theta \quad (21)$$

$$F_S=F_c\cos\theta+F_t\sin\theta \quad (22)$$

where θ denotes the angle between the fiber orientation and the trim plane.

Bhatnagar *et al.* (1995) showed that while the classical Merchant (1944) is applicable to homogeneous

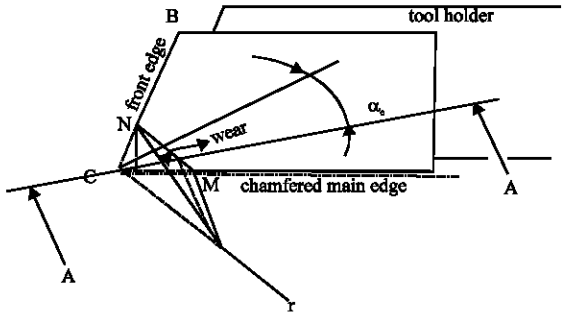

Fig. 4: Condition of tool tip wears with chamfered main cutting edge tool

methods and their alloys, he applies this model in the machining of FRP in the -θ cutting direction as a first approximation. He assumes the shear plane angle as the fiber angle where failure occurs. By substituting -θ for Ψ in Merchant's model, a basic relationship for the two components of the cutting force with the geometry of the cutting can be obtained:

$\tau_S = \tau_{compsite} = \tau_{fiber}\ V_f$ by Rosen and Dow (1987) (V_f is fiber contains):

$$V_S = V\cos\alpha_e / \cos(\varphi_e - \alpha_e) \tag{23}$$

$$f_t = \tau_S t_1 \sin\beta / \cos(\varphi + \beta - \alpha)\sin\varphi \tag{24}$$

where, f_t is the friction force in orthogonal cutting for unit width of cut and where, t_1 is the undeformed chip thickness (Fig. 1b):

$$V_C = V\sin\varphi_e / \cos(\varphi_e - \alpha_e) \tag{25}$$

$$\alpha_e = \sin^{-1}(\sin\alpha_{S2}\cos\alpha_b\cos\eta_C + \sin\eta_C\sin\alpha_b) \tag{26}$$

where, α_e is the effective rake angle; α_{S2} is the second normal side rake angle; α_b is the parallel back rake angle; ϕ_e is the effective shear angle equals to fiber orientation angle, θ (Hocheng *et al*., 1997); η_c is the chip flow angle which was determined that minimized the total cutting energy U; β is the mean friction angle by Merchant (1944); and τ_S is the shear stress by Rosen and Dow (1987). The cutting power is a function of at least α_b, α_{S1}, α_{S2}, d, W_e, C_S, C_e, f, V,θ_{ref}, θ, β, τ_S and η_c. The value of η_c for the total minimum power U_{min} to be used in Eq. 27 was obtained by calculating U for a range of values η_c according to the computer flow chart (Fig. 5). Therefore, $(F_H)_{Umin}$ was determined by solving Eq. 28 in conjunction with the energy method by Reklaitis *et al*. (1984):

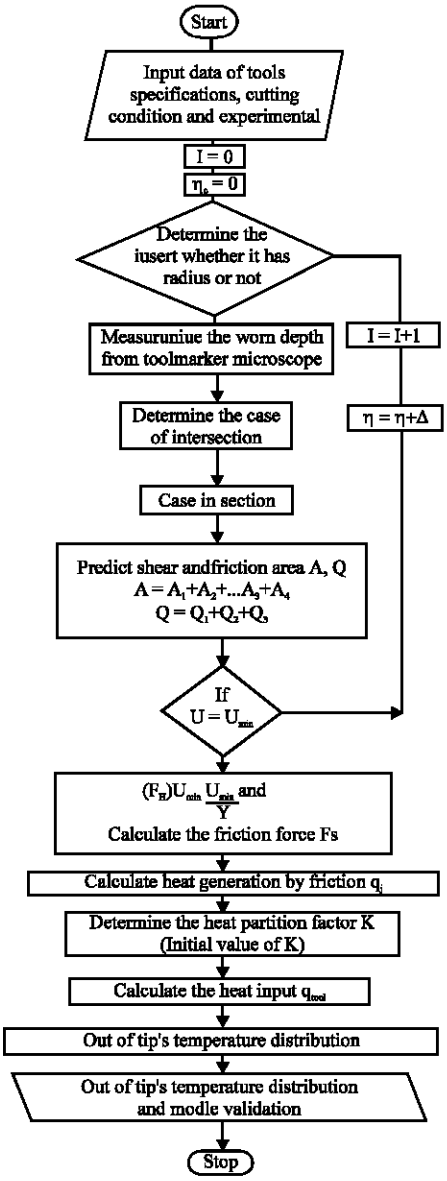

Fig. 5: Flow chart of the inverse heat transfer

$$U_{min} = (F_H)_{Umin} = F_H \tag{27}$$

$$F_H = \frac{U_{min}}{V} = \{\frac{\tau_S\cos\alpha_e A}{\cos(\phi_e - \alpha_e)} + \frac{\tau_S\sin\beta\cos\alpha_e Q}{\cos(\phi_e + \beta - \alpha_e)\cos(\phi_e - \alpha_e)} \tag{28}$$

where, the frictional force is determined by:

$$F_t = \frac{\tau_s\sin\beta\cos\alpha_e Q}{[\cos(\varphi_e + \beta - \alpha_e)\sin\varphi_e]} \tag{29}$$

where, N_t the normal force on the tip's surface with minimum energy where the frictional force is determined by:

$$N_t = \frac{[(F_H) - (F_t)_{U_{min}} \sin \alpha_e]}{\cos \alpha_{S2} \cos \alpha_b} \quad (30)$$

Calculation of flank wear: The tool tip wear is shown in Fig. 4. For simplification, the wear effects of front edge and main edge are omitted. The only effect to be controlled is the setting condition perpendicular to the vertical line. Thus, the flank wear V_B is a function of t_W, θ_e and α_e. The approximate flank wear is shown as follows:

$$V_B = t_W \cos \alpha_e (\cot \theta_e - \tan \alpha_e) \quad (31)$$

Solid modeling of carbide tip: The chamfered main cutting edge tool has a more complex geometry. To develop a 3D finite element model for thermal analysis, a solid model of the tip can be established in three steps. First, the Tip Cross-Section Profile (TCSP) perpendicular to the main cutting edge was measured using a microscope, then CAD software, SolidWorks™, was used to generate the tip body by sweeping the TCSP along the main cutting edge with the specified pitch. Finally the tip's main cutting edge was simulated to remove unwanted material and create a solid model of turning tip geometry, as shown in Fig. 6.

Finite element model: The finite element analysis software Abaqus™ is used in this study. The finite element mesh of the carbide tip is shown in Fig. 6 which was modeled by 58,000, four-node hexahedral elements. As shown in the top view of Fig. 6, 8*6 nodes are located on the projected contact length between the tool and the workpiece, 3*6 nodes are located on the chamfered width of the main cutting edge and 1*6 nodes are placed on flank wear. These should provide a reasonable solution in the analysis of tip temperature distribution in turning. The initial condition of finite element analysis has a uniform temperature of 25°C in the tip. Because the tip does not rotate in the experiment, free convection boundary condition is used when applied for the surface of tip contact with the workpiece.

Modified carbide tip temperature model: Magnitude of the tip's load is shown in the following Eq. 32 and 33:

$$K = U_f / A' \quad (32)$$

$$A' = L_p (d + W_e + V_b) \quad (33)$$

where, A' is the area of friction force action, U_f is the friction energy, W_e is the tip's chamfered width, d is the cutting depth, V_b is the flank wear of the tip and for simplification, the value of V_b is set to be 0.1 mm. L_f is the contact length between the cutting edge and the workpiece Eq. 19 L_p is the projected contact length between the tool and the workpiece, as referred to in Fig. 7 and can be determined by Eq. 20 and the following condition:

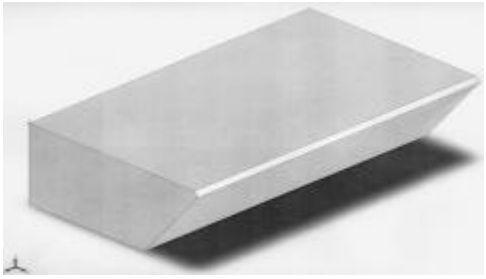

Fig. 6: Solid model of the chamfered edge tool

$$\rho c \frac{\partial T}{\partial t} = k \frac{\partial^2 T}{\partial x^2} + k \frac{\partial^2 T}{\partial y^2} + k \frac{\partial^2 T}{\partial z^2} \quad (34)$$

where, ρ is the density, c is the thermal conductivity and k is the heat capacity.

The boundary condition on the square surface at the cutting edge, opposite from the turning tip, also assumed to be maintained in turning, is assigned to be 25°C. The heat generation in turning is applied as a line load on the main cutting edge. The contact between tool and chip is wide in stainless steel machining according to Eq. 19 to 20. Compared to the 0.36 mm feed per revolution, the characteristic length of the elements at tip and cutting edges is much larger, around 3.29 mm. This allows the use of line heat flux at the cutting edge in finite element analysis. The heat generation assuming the cutting edge is perfectly sharp, the friction force, and the chip velocity are multiplied to calculate the line heat generation rate, q_f, on cutting edge $q_f = F_f V_c$.

Assuming K is the heat partition factor to determine the ratio of heat transferred to the tool, the heat generation rate q_{tool} on each cutting edge is given by Li and Shih (2005):

$$q_{tool} = K q_f \quad (35)$$

In this study, K is assumed to be a constant for all cutting edges. The inverse heat transfer method is used to find the value of K under certain turning speeds.

Inverse heat transfer solution and validation: The flowchart for inverse heat transfer solution of K was obtained by the Abaqus™ solver and is summarized in

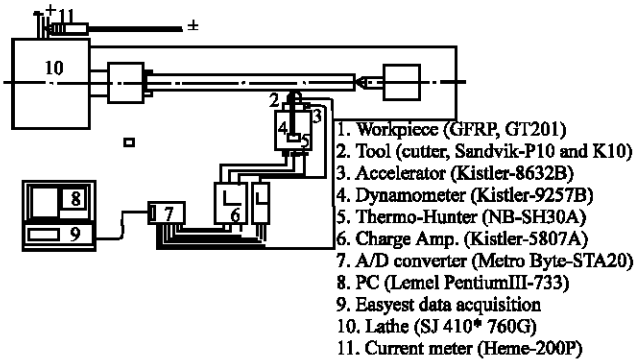

Fig. 7: Experimental set-up

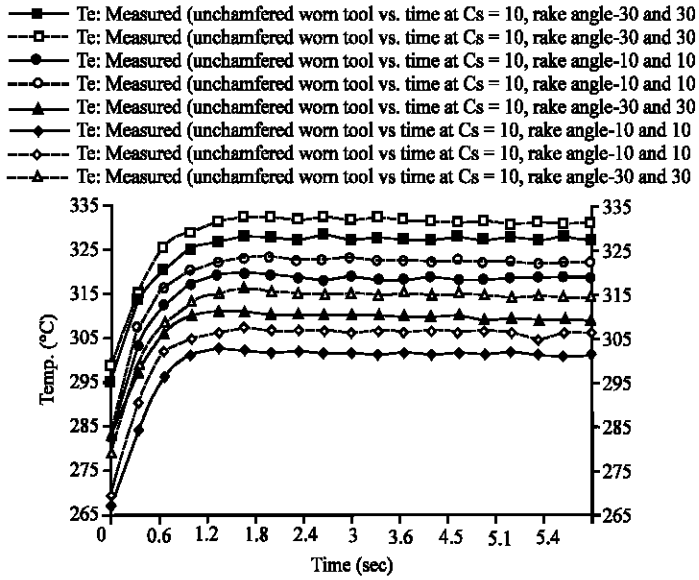

Fig. 8: Cutting temperatures versus cutting time for different values α_{S1} and α_{S2} with unchamfered and chamfered sharp tool at d = 3.0 mm, f = 0.33 mm rev^{-1}, V = 252 m min^{-1} and C_s = 30° (CFRP)

Fig. 5. By assuming a value for K, the spatial and temporal temperature distribution of the tip can be found. The inverse heat transfer method is applied to solve K by minimizing an energy function on the tip surface determined by Eq. 35-36 and finite element modeled temperature at specific infrared locations, as shown in Fig. 7 on the tip face. Using an estimated value of K, the heat generation rate is calculated and applied to nodes on the tip's main and end cutting edges. The discrepancy between the experimentally measured temperature by infrared pyrometer, j by time t_i, $T^{ti}_j|$ and finite element estimated temperature at the same infrared location and time, $T^{ti}_j|$ determines the value of the objective function by Li and Shih (2005):

$$Obj(K) = \sum_{i=1}^{n_i}\sum_{j=1}^{n_j}(T_j^{ti}\big|_{exp} - T_j^{ti}\big|_{est})^2 \qquad (36)$$

where, n_i is the number of time instants during turning and n_j is the number of thermocouples selected to estimate the objective function.

After finding the value of K, the finite element model can be used to calculate temperature at locations of thermocouples not used for inverse heat transfer analysis. The tool tip's temperature predicted from finite element model is compared with experimental measurements to validate the accuracy of proposed method.

EXPERIMENTAL PROCEDURES

Experimental set up is shown in Fig. 7. Workpiece is observed in Fig. 7. to be held in the chuck of a lathe and the cutters that were mounted with a dynamometer were employed for measuring the three axes compound of forces (F_H, F_V and F_T).

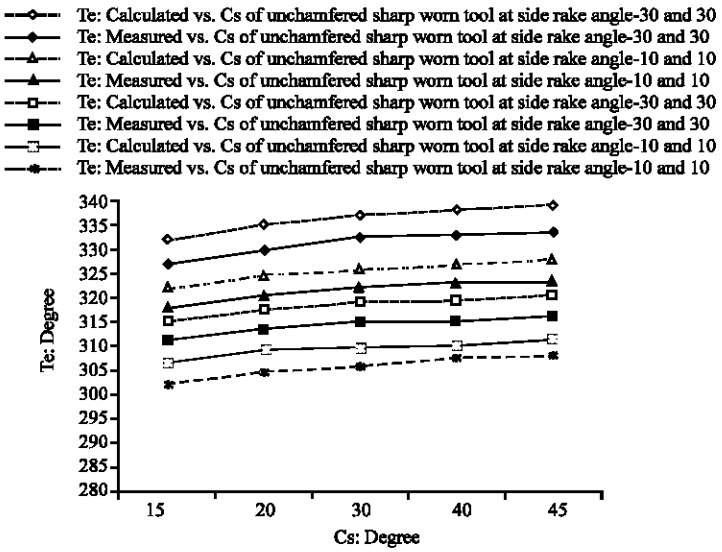

Fig. 9: The cutting temperatures vs. C_s for different values α_{S1} and α_{S2} with chamfered and unchamfered sharp tool at d = 3.0 mm, f = 0.33 mm rev^{-1}, V = 252 m min^{-1}, respectively.

Table 2: Properties of the work materials (roving continuous strand, hardness, HS: 55~60)

Density g cm^{-3}	Thermal conductivity (kCal hr^{-1}°C)	Fiber content	Thermal expansion (10^{-6}/°C)	Tensile strength (kg cm^{-2})	Compressive strength (kg cm^{-2})	Shear strength (kg cm^{-2})	Modulus tensile (kg cm^{-2})
1.7~1.9	0021~0.28	75%	2~9	3.5~4	3.5~3.9	1.5~2	235~400

The work material used was 0°; unidirectional filament wound fiber of CFRP with Vinylester resin composite materials in the form of bars having a diameter of 40 and 500 mm length by Liu (2002). Table 2 shows some of the physical and mechanical properties of CFRP prior to carrying out the cutting experiments. The cutting tools used in the experiments are Sandvik H1P (K type) by Brookes (1992). Carbide-tipped tools with following angles are used: back rake angle = 0°; side rake angle = 6°; end relief angle =7°; side relief angle = 9°; end cutting edge angle = 70°; side cutting angle = 20, 30, 40° and nose radius = 0, 0.1 mm. Tool composition: WC 85.5%, TiC 7.5%, Ta (Nb)C 1% and Co 6% (30), HV = 1850, density = 12.9 g cm^{-1}, thermal conductivity = 60W/m-°K and heat capacity = 235 J/kg-°K. Oblique turning tests were carried out for each tool. The experimental tests are as follows: dry cutting; cutting velocity equals to 252 m min^{-1}; cutting depth equals to 3.0 mm; feedrate equals to 0.33 mm rev^{-1}. Block diagrams of performance are drawn as shown in Fig. 5. The cutting force, cutting temperature was observed and discussed.

RESULTS AND DISCUSSION

The cutting forces: Chang demonstrated in turning of CFRP with chamfered main cutting edge sharp tools, the resultant cutting force, Fr, is about 15% less than that for unchamfered main cutting edge sharp tools (Chang, 2006a). As well as in the case of turning CFRP with chamfered main cutting sharp worn tools, it shows the theoretical cutting forces are good agreement with the experimental values.

Temperature of surface of tip: Inverse heat transfer utilizes the temperature measured by infrared on the surface of tip as the input to predict the heat flux on the chamfered main cutting edge tools. This method determines the heat partition factor using the optimization method. Knowing the temperature of cutting tools (Fig. 6) and how this chamfered main cutting edge tools decreases the temperature of the tool tip surface, as indicated in the following: Based on Li and Shih (2005), according to Eq. 34-35, the flowchart for inverse heat transfer solution of K is described in Fig. 5. After finding the value of K, the finite element model can be applied to calculate temperature at tips, the results are shown in Fig. 8-10. Figure 8 and 9 show the cutting temperatures vs cutting time for different values α_{S1} and α_{S2} with chamfered and unchamfered sharp tool at C_s = 30°. Figure 9 shows temperature distribution with chamfered cutting edge inserts (a) heat flux (b) near the tool nose at C_s = 30, α_{S1} = -30° and α_{S2} = 30°, d = 3.0 mm, f = 0.33 mm rev^{-1} and V = 252 m min^{-1} (CFRP).

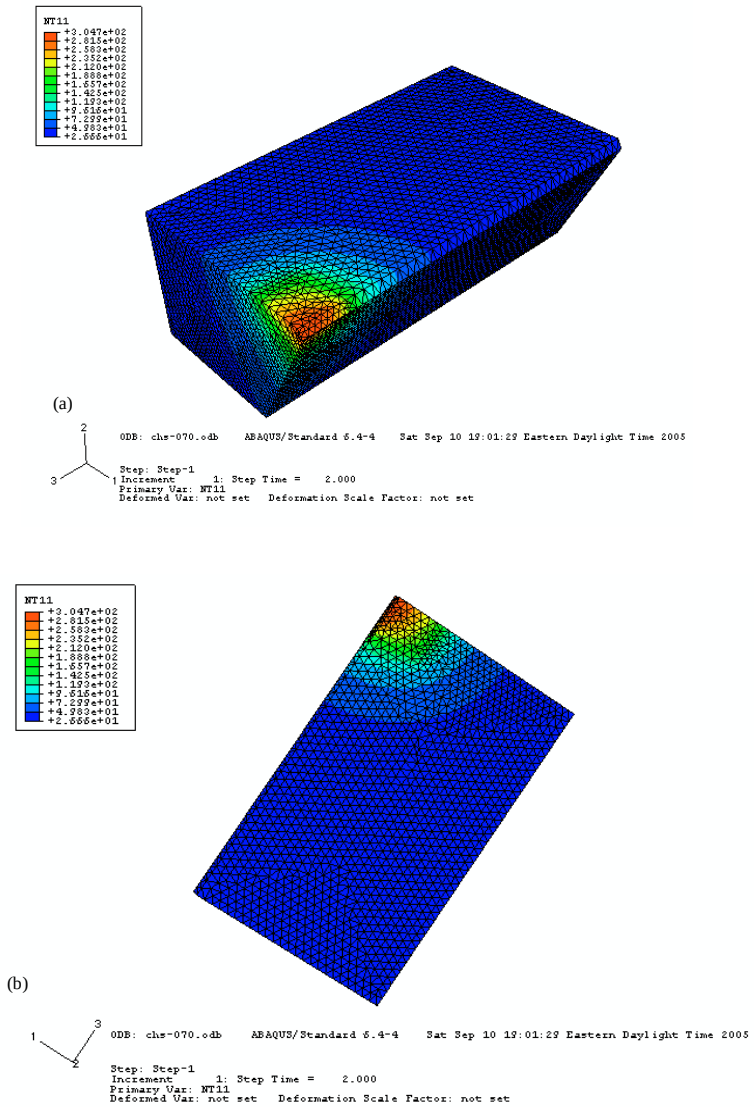

Fig. 10: Temperature distribution with chamfered cutting edge inserts (a) heat flux (b) near the tool nose at C_S = 30°, $\alpha_{S1}(\alpha_{S2})$, = -10°(10°) d = 3.0 mm, f = 0.33 mm rev^{-1} and V = 252 m min^{-1} (CFRP)

- From Fig. 8, it proved that the cutting edge temperature of the chamfered main edge tool was lower than unchamfered main cutting edge tool
- According to Fig. 8-9, the tip temperatures of chamfered main cutting edge tool were not high and the inverse (calculated) data correlates closely with the experimental values
- From Fig. 8, it proved that the distribution of chamfered main cutting edge tool's temperature was close the Fig. 10

CONCLUSIONS

A series of preliminary tests were conducted to asses the effect of tool geometries of K type of chamfered main cutting edge carbide tool. Chamfered cutting edge sharp worn tools with C_S = 20°, the conditions f = 0.24 mm rev^{-1}, $\alpha_{S1}(\alpha_{S2})$ = -10°(10°) and nose radius R = 0.3 mm, produce the lower cutting forces and lower cutting temperature. Good correlations between predicted values and experimental results of forces and temperatures during machining with sharp worn tools in cutting CFRP. The

FEM and Inverse heat transfer solution in tool temperature in CFRP turning is obtained and compared with experimental measurements. The good agreement demonstrates the proposed model.

APPENDIX A

Coefficients of the tool have a sharp corner (R = 0) without tool wear:

$$a_1 = [(f\cos C_s - W_e\cos\alpha_{s1})(\tan\eta_c - \tan(C_e - C_s)) (1/\cos\alpha_e + 1/\cos\eta_c - 2\sin\alpha_b/\cos\alpha_e\cos\eta_c)^{1/2} \quad (1)$$

$$b_1 = \frac{(f\cos C_3 - W_e\cos\alpha_{S1})}{\cos\eta_c\sin\phi_e} \quad (2)$$

$$c_1 = \frac{(f\cos C_s - W_e\cos\alpha_{S1})}{\cos\alpha_e\cos\eta_c} \quad (3)$$

$$a_2 = \frac{d}{\cos C_s\cos a_b} \quad (4)$$

$$b_2 = (d/\cos C_s\cos\alpha_b - (f\cos C_s - W_e\cos\alpha_{s1}/\cos\alpha_e) [\tan\eta_c - \tan(C_e - C_s)] \quad (5)$$

$$h_2 = (f\cos C_s - W_e\ \alpha_{S1})\left(\frac{1}{\cos^2\eta_c\sin^2\phi_e} - \frac{1}{\cos^2\alpha_e}\right)^{1/2} \quad (6)$$

APPENDIX B

Coefficients of the tool have a sharp corner (R = 0) with tool wear:

$$a_3 = \{[\frac{f\cos C_s}{\cos\alpha_{S2}} - W_e\cos\alpha_{S1} - \overline{CN}\cos(C_e - C_s)]^2[\tan\eta_c - \tan(C_e - C_s)]^2 + (f\cos C_s/\cos\alpha_e - W_e\cos\alpha_{s1} - \overline{CN}\cos(C_e - C_s))/\cos\eta_c]^2(\cos^2\alpha_e \frac{(\frac{f\cos C_s}{\cos\alpha_e} - W_e\cos\alpha_{S1} - \overline{CN}\cos(C_e - C_s))}{\cos\eta_c}]^2(\cos^2\alpha_e(\tan\alpha_e + \cot\phi_e)^2 - 2[(f\cos C_s/\cos\alpha_e - W_e\cos\alpha_{s1} - \overline{CN}\cos(C_e - C_s))/\cos\eta_c] \cos\alpha_e(\tan\alpha_e + \cot\phi_e)\cos(0.5\pi - \alpha_b)\}^{1/2} \quad (1)$$

$$b_3 = [\frac{\frac{f\cos C_s}{\cos\alpha_{S2}} - W_e\cos\alpha_{S1} - \overline{CN}\cos(C_e - C_s)}{\cos\eta_c}]\frac{\cos\alpha_e}{\sin\phi_e} \quad (2)$$

$$c_3 = [\frac{f\cos C_s/\cos\alpha_{s2} - W_e\cos\alpha_{s1})}{\cos(C_e - C_s)} - \overline{CN} \quad (3)$$

$$a_4 = d/\cos C_s - [f\cos C_s/\cos\alpha_{s2} - W_e\cos\alpha_{s1} - \overline{CN}\cos(C_e - C_s)]^2 [\tan\eta_c - \tan(\eta_c - \tan(C_e - C_s)) - \overline{NM}\sin (\pi - \angle CMN - \theta_B - \eta_c - C_e - C_s)/\sin(\theta_B - \eta_c + C_e - C_s) \quad (4)$$

$$b_4 = d/(\cos C_s - \cos C_e) - \overline{CM} \quad (5)$$

$$h_4 = (c_4^2 - d_4^2)^{1/2} \quad (6)$$

$$c_4 = [\frac{f\cos C_s - W_e\cos\alpha_{s1} - \overline{CN}\cos(C_e - C_s)}{\cos\eta_c} + [\frac{\overline{NM}\sin(\pi - \theta_B - \angle CNM)}{\sin(\theta_B - \eta_c + C_s - C_e)}]\frac{\cos\alpha_e}{\sin\phi_e} \quad (7)$$

$$a_5 = \overline{NM}\ b_5 = b_5\ c_5 = a_3$$
$$e_5 = [\frac{f\cos C_s}{\cos\alpha_{S1}} - W_e\cos\alpha_{S1} - \overline{CN}\cos(C_e - C_s)][\tan\eta_c - \tan(C_e - C_s)] \quad (8)$$

$$d_5 = [\frac{(\frac{f\cos C_s}{\cos\alpha_e} - W_e\cos\alpha_{S1} - \overline{CN}\cos(C_e - C_s)}{\cos\eta_c}]\cos\alpha_e(\tan\alpha_e + \cot\phi_e) \quad (9)$$

$$g_5 = [\frac{f\cos C_s/\cos\alpha_{s2} - W_e\cos\alpha_{s1} - \overline{CN}\cos(C_e - C_s)}{\cos\eta_c} + [\frac{\overline{NM}\sin(\pi - \theta_B - \angle CNM)}{\sin(\theta_B - \eta_c + C_s - C_e)}]\frac{\cos\alpha_e}{\sin\phi_e} \quad (10)$$

$$h_5 = (m_5^2 + n_5^2 - 2m_5n_5\sin a_b)^{1/2} \quad (11)$$

$$m_5 = \frac{\overline{NM}\sin(\pi - \theta_B - \angle CNM + \eta_c - C_e + C_s)}{\sin(\theta_B - \eta_c + C_e - C_s)} \quad (12)$$

$$n_5 = g_5\sin\phi_e(\tan\alpha_e + \cot\phi_e) - d_5$$
$$l_5 = [\frac{f\cos C_s}{\cos\alpha_{S1}} - W_e\cos\alpha_{S1} - \overline{CN}\cos(C_e - C_s)][\tan\eta_c - \tan(C_e - C_s)) - \quad (13)$$

$$\overline{CM} + \frac{\overline{NM}\sin(\pi - \theta_B - \angle CNM + \eta_c - C_e + C_s)}{\sin(\theta_B - \eta_c + C_e - C_s)} \quad (14)$$

$$s_5 = (l_5^2 + r_5^2 - 2l_5r_5\sin a_b)^{1/2} \quad (15)$$

$$r_5 = g_5\sin\phi_e(\tan\alpha_e + \cot\phi_e)/\cos\alpha_e \quad (16)$$

ACKNOWLEDGMENT

This work was supported by National Science Council, Taiwan, R.O.C. under grant number NSC 2009-2622-E-197-001-CC3

REFERENCES

Bhatnagar, N., N. Ramakrishnan, N.K. Naik and R. Komanduri, 1995. On the machining of Fiber Reinforced Plastic (FRP) composite laminates. Int. J. Mach. Tools Manuf., 35: 701-716.

Brookes, K.J., 1992. World Directory and Handbook of Hard Metals. 5th Edn., International Carbide Data Hand Book, UK., ISBN-13: 9780950899527, pp: 172-175.

Chang, C.S., 2006a. Turning of glass fiber reinforced plastics materials with chamfered main cutting carbide tools. J. Mater. Process. Technol., 180: 117-129.

Chang, C.S., 2006b. Turning of CFRP composites using chamfered main cutting edge tools. J. Mach. Sci. Technol., 180: 117-129.

Chang, C.S., 2008. Prediction of cutting temperatures in turning of glass-fiber reinforced plastics with chamfered main cutting edge tools. J. Mech., 24: 241-252.

Ferreira, J.R., N.L. Coppini and F.L. Neto, 2001. Characteristics of carbon-carbon composite turning. J. Mater. Process. Technol., 109: 57-71.

Hocheng, H., H.Y. Tsai, J.J. Shiue and B. Wang, 1997. Feasibility study of abrasive waterjet milling of fiber-reinforced plastics. J. Manuf. Sci. Eng., 119: 133-142.

Li, R. and A.J. Shih, 2005. Inverse heat transfer solution in tool temperature titanium drilling, mechanical engineering. University of Michigan, Ann Arbor, MI., USA.

Liu, C.C., 2002. FRP and GTI composites. Golden Talent Industries Co. Ltd., Hsin-Chu, Taiwan.

Malhotra, S.K., 1990. Some studies on drilling of fibrous composite. J. Mater. Process. Technol., 24: 291-300.

Merchant, M.E., 1944. Basic mechanics of the metal cutting process. Transactions ASME, 66: 65-71.

Reklaitis, G.V., A. Ravindran and K.M. Ragsdell, 1984. Region-Elimin Method, Engineering Optima: Methods and Application. Wiley-Interscience Press, New York, USA., pp: 37-38.

Rosen, B.W. and N.F. Dow, 1987. Overview of Composite Materials, Analysis and Design. In: Engineered Materials Handbook: Composites, Reinhart, T.J. (Ed.). Vol. 1. American Society for Metals, USA., ISBN-13: 9780871702791, pp: 175-180.

Shamoto, E. and Y. Altintas, 1999. Prediction of shear angle in oblique cutting with maximum shear stress and minimum energy principles. J. Manuf. Sci. Eng., 121: 399-407.

Singamneni, S.B., 2005. A mixed solution for the three-dimensional temperature distribution in turning inserts using finite and boundary element techniques. J. Mater. Process. Technol., 166: 98-106.

Takeyama, T.H. and R. Murata, 1963. Basic investigation of tool wear. J. Eng. Ind., 85: 33-38.

Wang, D.H., M. Ramulu and D. Arola, 1995. Orthogonal cutting mechanisms of graphite/epoxy composite. Part I: Unidirectional laminate. Int. J. Mach. Tools Manuf., 35: 1623-1638.